Digital Discovery

Accepted Manuscript

Digital Discovery

Volume 1
Number 1
January 2022

rsc.li/digitaldiscovery

ISSN 2635-098X

ROYAL SOCIETY
OF CHEMISTRY

ROYAL SOCIETY
OF CHEMISTRY

rsc.li/digitaldiscovery

Journal Name

ARTICLE TYPE

Efficient Symmetry-Aware Materials Generation via Hierarchical Generative Flow Networks

Tri Minh Nguyen [1], Sherif Abdulkader Tawfik [1], Truyen Tran [1], Sunil Gupta [1], Santu Rana[1], Svetha Venkatesh [1]

Discovering new solid-state materials requires rapidly exploring the vast space of crystal structures and locating stable regions. Generating stable materials with desired properties and compositions is extremely difficult as we search for very small isolated pockets in the exponentially many possibilities, considering elements from the periodic table and their 3D arrangements in crystal lattices. Materials discovery necessitates both optimized solution structures and diversity in the generated material structures. Existing methods struggle to explore large material spaces, outside the training space, and generate diverse samples with desired properties and requirements. We propose the Symmetry-aware Hierarchical Architecture for Flow-based Traversal (SHAFT), a novel generative model employing a hierarchical exploration strategy to efficiently exploit the symmetry of the materials space to generate crystal structures given desired properties. In particular, our model decomposes the exponentially large materials space into a hierarchy of subspaces consisting of symmetric space groups, lattice parameters, and atoms. To benchmark our approach, we first develop a novel, non-hierarchical GFlowNet for complete crystal structure generation. We then introduce SHAFT, a more expressive hierarchical model that leverages its architecture and increased model capacity to more efficiently explore the materials space. We demonstrate that SHAFT significantly outperforms the flat GFlowNet baseline and other state-of-the-art methods like CDVAE and DiffCSP in generating valid, stable, and diverse crystal structures.

1 Introduction

Discovering new solid-state materials plays a central role in advancing multiple critical industries, including energy generation and storage, and semiconductor electronics [1,2]. Each unique crystal structure exhibits properties useful for specific applications. For example, superconductive perovskite structure is used in circuit board elements for computers. Generating material structures that meet given property requirements poses a set of unique challenges. The key challenge is generating crystal structures that exhibit a repeating arrangement of atoms in three-dimensional space. A crystal structure is determined by how atoms are arranged within the unit cell specified by their lengths and angles. However, the inter-atom interactions are not confined within the unit cell but also with adjacent unit cells. These characteristics make the search space of crystal structures significantly larger and more complex compared to well-studied molecular search space. The number of known crystal structures, both experimental and hypothetical, is around 3 million curated from AFlow [3–5] and Material Project [6],

which is tiny compared to billions of molecules from the Zinc dataset [7]. The limited data undermines modern data-driven methods to learn the crystal structure representation [8,9].

We address the complexity associated with the large search space by proposing a new generative model termed Hierarchical Symmetry-aware Hierarchical Architecture for Flow-based Traversal (SHAFT). SHAFT explores the vast search space in an efficient way. The key insight to solving the large state space problem is breaking space exploration into more meaningful hierarchical sub-tasks. Here the higher-level tasks explore more actions that are closely related to the reward function, while lower-level tasks handle the configuration adjustment corresponding to the action taken at higher-level tasks. Since the exploration starts at the highly general concept level, it can learn a more meaningful policy that corresponds to the target reward function. With more meaningful actions taken at a higher level, the policy networks can focus on searching the actions in a significantly smaller sub-space that corresponds to actions of high-level tasks instead of exploring the whole space.

Three key concepts can help generative models search the material space effectively. First, the crystal structure class imposes symmetry operations and geometrical characteristics on atom posi-

^{a} *Applied Artificial Intelligence Institute, Deakin University. Address: 75 Pigdons Rd, Waurn Ponds VIC, Australia. E-mail: tri.nguyen1@deakin.edu.au, s.abbas@deakin.edu.au, truyen.tran@deakin.edu.au, sunil.gupta@deakin.edu.au, santu.rana@deakin.edu.au, svetha.venkatesh@deakin.edu.au*
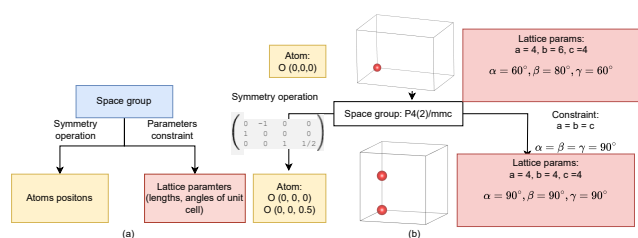
Fig. 1 (a) Hierarchical crystal structure state. The space group level provides the set of symmetry operations for atoms' positions and lattice parameters constraints. (b) An example of applying the hierarchical state space. The current state has one Oxygen atom at position (0, 0, 0), lattice parameters $a = 4, b = 6, c = 4, \alpha = 60°, \beta = 80°, \gamma = 60°$, and $P1$ spacegroup. The action of choosing space group P4(2)/mmc provides a symmetry operation to generate another Oxygen atom at position (0, 0, 0.5). The lattice parameter constraints reduce the unit cell's length search space from $\mathbb{R}^3$ to $\mathbb{R}$ and make the unit cell's angles constant at $90°$

tions and lattice parameters, as seen in Fig. 1, effectively reducing the material search space. Second, searching for stable structures on the non-smooth energy landscape defined by quantum mechanics requires generative models to explore and generate diverse sample sets. This approach helps avoid getting stuck in a single mode or local minima. Third, we apply bond constraints on atom pairs in the generated crystals, ensuring atoms are not closer to each other than specific bond thresholds. These thresholds are obtained using all materials in the Materials Project database. Given the diversity of materials in this database, it's reasonable to assume that minimum distances derived from it are threshold distances for the ground state structure of the respective atoms in any new crystal structure. By incorporating these concepts, generative models can more effectively navigate the complex material space and produce stable, diverse, and physically realistic crystal structures.

We model the entire material space in a hierarchical structure. The highest level is the crystal structure class, which is related to relevant material properties. Exploring this class can efficiently lead to more optimal properties of the generated structure. Specifically, we use the space group of the crystal structure to effectively reduce the 3D atom space exploration to a more meaningful high-level exploration and generate a high-symmetry crystal structure. The next level searches for the unit cell lattice parameters and atom configurations given the space group. The space group imposes constraints on these parameters and atom positions, thus reducing the search space. Choosing positions one by one creates a long-horizon trajectory, making it difficult to learn a policy that generates high-symmetry structures proportional to the reward function. By leveraging the space group's symmetry operations, we can immediately replicate atoms over the unit cell. This approach reduces the trajectory length, making it easier for the policy network to learn how to generate a high-symmetry crystal structure.

While deep generative models have shown promise, the immense complexity and size of the material search space remain a formidable barrier. Prior methods using Generative Flow Networks (GFlowNets), such as Crystal-GFN [10], have successfully generated crystal parameters like space groups and lattice constants, but stop

short of generating the complete crystal structure, omitting the explicit placement of atoms. Our work addresses this complete generation problem.

Our work first addresses this complete generation problem by developing a novel, non-hierarchical or "flat," GFlowNet that generates the full crystal-space group, lattice, and atomic coordinates within a single, monolithic policy framework. This in itself is a significant advance for creating full atomic structures with GFlowNets. However, we hypothesize that such a flat approach struggles to efficiently navigate the intricate, long-horizon dependencies inherent in crystal design. To overcome this, we then introduce SHAFT, a hierarchical model that decomposes the generation problem to improve learning efficiency and exploration. The comparison between SHAFT and our flat GFlowNet baseline is therefore designed specifically to isolate and quantify the benefits of this hierarchical decomposition.

Our main contributions are:

>We propose a generative model that can search effectively in a large search space, even outside the observed training dataset space, by modeling the state space in a hierarchical structure.

>We incorporate the physical knowledge curated from the large material databases into our generative model to generate more stable structures.

>We validate the hierarchical structure state space and physics priors of our proposed generative model in the crystal structure generation task to show the efficiency in material space exploration as well as the stability of the generated structures.

2 Related Works

There are three main approaches to crystal structure generation. >The first is **Element Substitution**: Given a crystal template [11], the elements are substituted with other elements having similar properties [12–14]. This approach is computationally expensive and relies on domain knowledge in element substitution. >The second strategy is **Distribution Sampling**: Deep generative models learn from the distribution of known stable crystal structures to sample new structures, such as those by Variational AutoEncoders (VAEs) [2,15,16], Generative Adversarial Networks (GANs) [17,18], symmetry-aware Diffusion Models [19], and periodic-E(3)-equivariant denoising model [20]. Recent advances in generative modeling for materials design include SymmCD's symmetry-preserving crystal generation [21], GNoME's large-scale discovery of stable inorganic materials using graph neural networks [22], and MatterGen's diffusion-based model capable of generating novel [23], stable materials under diverse structural and property constraints. This data-driven approach has difficulty in generating high symmetry structures and in out-of-distribution generalization. Most sampled crystal structure. Also, the generation process is solely based on learning from the known data, leaving minimal room for domain knowledge and human intervention during the generation process. And finally, >**Iterative Generation**: Crystal structures can be decomposed into compositional objects, and constructed step by step using reinforcement learning (RL) [24]. Crystal-GFN [10] uses GFlownet to generate crystal structures' parameters such as space group, lattice lengths, and angles, but it does not generate the complete structure with atoms'

coordinates. Crystal-GFN uses GFlowNet to determine crystal parameters via a fixed, linear sequence of actions (space group, then composition, then lattice parameters), but it does not generate the complete structure with atoms' coordinates. This contrasts with our framework, which employs an iterative refinement process where the space group, lattice, and atomic placements can be dynamically updated throughout the generation trajectory. Our work is the first to apply the RL-based technique to explore the entire material and atom space. The key advantage of this RL-based approach is that it allows the incorporation of domain knowledge into the action and state space and shaping the reward function. The RL can generalise to **Hierarchical RL** which solves the long horizon trajectory problem by designing sub-goals[25,26]. By exploiting high-level crystal structure classes such as space groups, SHAFT creates a sub-goal for low-level policies, helping them to learn the atom coordinates space more effectively.

Generative Flow Networks (GFlowNet) are generative models designed to sample candidates proportional to their target rewards. The framework has been successfully applied to many fields such as molecular discovery[27], protein sequence discovery[28], causality[29], and continuous control[30]. Jiangyan et al.[31] integrate symmetries into GFlowNets with equivalent actions. LS-GFN[32] explores the local neighborhood to avoid the over-exploration in GFlownet. Our SHAFT is a generalization of GFlowNets for more efficient sampling by modelling the hierarchy of the search space. When applied to crystal structure generation, SHAFT also exploits the group symmetry unique to this domain.

3 Preliminaries

3.1 Crystallographic Space Group

The crystal structure is the repeating arrangement of the atoms within a unit cell in 3D. Formally, the unit cell of N atoms is a triplet (L, A, X) of lattice parameters L, atom list A, and atom coordinates X. There are 6 lattice parameters $L = (a, b, c, \alpha, \beta, \gamma) \in \mathbb{R}^6$ describing 3 lengths and 3 angles of the unit cell, respectively. The atoms list $A = (a_1, ..., a_N)$ describes the elements. The atoms' coordinates $X \in \mathbb{R}^{N \times 3}$ describe the positions of the atoms within the unit cell, which can be Cartesian or fractional.

The space group of crystal structure consists of a list of symmetry transformations to the atoms within the unit cell. In crystallography, there are 230 space groups[33]. Each space group has geometrical characteristics defined in lattice angles and lengths that can be used as constraints to limit the parameters search space. The list of geometrical characteristics is provided in the Appendix S1. Given the space group G_s, the elements of the space group $g \in G_s$ are a set of symmetry operations. A crystallographic orbit of an atom $o = (x_o, a_o)$ with coordinate x_o and element a_o is defined as $O_{G_s}(x_o) = \{g \cdot x_o \mid g \in G_s\}$, where $g \cdot x_o$ denotes the application of the symmetry operation g on the atom o within the unit cell. From a reference atom o, we can obtain a set O_{G_s} of equivalent points.

3.2 Generative Flow Network

GFlowNet models the sampling process of the compositional object s as the directed acyclic graph (DAG) $G = (S, A)$ where S is the

set of states and A is the state transition which is the subset of $\mathscr{S} \times \mathscr{S}$. The sampling process starts with the initial state vertex $s_0 \in S$ with no incoming edge. and stops at the sink state vertex $s_n \in S$, n is the sampling trajectory length, with no outgoing edge. GFlowNet learns a policy function π that can sample the object x with the probability proportional to the non-negative reward function. GFlowNets constructs the object step by step, from the initial state s_0 to the sink state s_n, forming a trajectory $\tau = s_0, .., s_n, \tau \in \mathcal{T}$ where $\mathcal{T}$ is the trajectory set. For any state s in the trajectory, we can define the flow of the state as $F(s) = \sum_{\tau \ni s} F(\tau)$ and the flow of the edge $s \to s'$ as $F(s) = \sum_{\tau \ni s \to s'} F(\tau)$[27]. The forward policy that maps the probability of transition from the current state s to the next state s' is given as $P_F(s'|s) = \frac{F(s \to s')}{F(s)}$. The backward policy mapping probability transition to the previous state s given the current state s' is $P_B(s|s') = \frac{F(s \to s')}{F(s')}$. The training objective of the GFlowNets is flow matching consistency where the incoming flow is equal to the outgoing flow, $\sum_{s'' \to s} F(s'' \to s) = F(s) = \sum_{s \to s'} F(s \to s')$, for all states.[34] propose trajectory balance to deal with the long trajectory credit assignment problem. Given the trajectory $\tau = (s_0 \to s_1 \to ... \to s_n)$, the forward probability of a trajectory is defined as $\prod_{t=1}^n P(s'|s)$. The trajectory balance constraint is defined as:

$$Z \prod_{t=1}^n P_F(s_t|s_{t-1}) = F(x) \prod_{t=1}^n P_B(s_{t-1}|s_t) \tag{1}$$

where $P(s_n = x) = \frac{F(x)}{Z}$, $Z = F(s_0)$ is the initial state flow. Then the trajectory balance objective is defined as:

$$\mathscr{L}_{TB}(\tau) = \left(\log \frac{Z_\theta \prod_{t=1}^n P_F(s_t|s_{t-1}; \theta)}{R(x) \prod_{t=1}^n P_B(s_{t-1}|s_t; \theta)} \right)^2 \tag{2}$$

4 Methods

To best leverage the group symmetry in the crystal structure space, here we propose SHAFT (Symmetry-aware Hierarchical Architecture for Flow-based Traversal), a generic flow-based generative model that explores the space in a hierarchical manner. In SHAFT, the lower states represent discrete concepts constrained by the higher states that represent more abstract concepts. When applied to crystal structure generation, SHAFT makes use of the group symmetry in the space. See Fig. 1 for the overall structural state design.

4.1 Hierarchical Policy

A standard, or "flat," GFlowNet-based approach to crystal generation would treat the entire process as a single sequence of actions managed by one monolithic policy network. This policy would be responsible for every decision, from selecting a space group to specifying the precise fractional coordinates of each atom. While feasible, this approach faces significant challenges: it must learn the complex interplay between all degrees of freedom simultaneously from a unified and vast action space. The critical, high-level decision of choosing a space group is diluted among many low-level, continuous decisions, making it difficult for the agent to attribute a high final reward to a good initial space group choice.

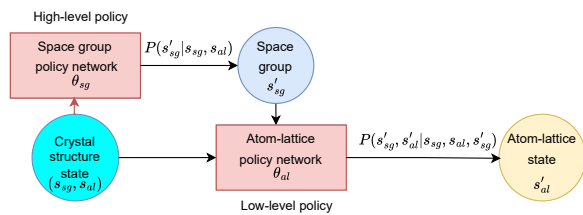To address this, SHAFT introduces a hierarchical policy structure

Fig. 2 Hierarchical policy for crystal structure state. First, the crystal structure graph state s is decomposed into space group state s_{sg} and atom-lattice state s_{al}. Then the transition probability $P(s'_{sg}|s_{sg},s_{al})$ in Eq. 4 is given by the space group policy network θ_{sg}. The transition probability $P(s'_{al}|s_{sg},s_{al},s'_{sg})$ in Eq. 4 is given by the atom-lattice policy network θ_{al}.

that decomposes the generation process into two distinct, more manageable sub-tasks, as illustrated in Figure 2. This design is motivated by the natural hierarchy present in crystal structures themselves. SHAFT generalises GFlowNets to accommodate a policy hierarchy of two levels: The high-level decision-making policy operating on the space groups, and the low-level execution policy operating on the atom-lattices (see Fig. 2). The space group policy chooses the space group and applies corresponding constraints on the atom-lattice policy actions. The corresponding hierarchical state space is decomposed as $s = (s_{sg}, s_{al})$, where s_{sg} is the space group state and s_{al} is the atom-lattice state. The latter consists of lattice parameters s_{lp}, atoms' coordinate s_{ac}, and atoms' type s_{at} states.

Then we define the probability of transitions as:

$$P(s'|s) = P(s'_{sg}, s'_{al}|s_{sg}, s_{al}) \tag{3}$$

$$P(s'_{sg}, s'_{al}|s_{sg}, s_{al}) = P(s'_{al}|s_{sg}, s_{al}, s'_{sg})P(s'_{sg}|s_{sg}, s_{al}) \tag{4}$$

Then given the trajectory $\tau = (s_0 \rightarrow s_1 \rightarrow ... \rightarrow s_n)$, we then have the trajectory balance constraint (Eq. 1) with the decomposed state as:

$$Z \prod_{t=1}^{n} P_F(s^t_{al}|s^{t-1}_{sg}, s^{t-1}_{al}, s^t_{sg})P_F(s^t_{sg}|s^{t-1}_{sg}, s^{t-1}_{al}) \tag{5}$$

$$= F(x) \prod_{t=1}^{n} P_B(s^{t-1}_{al}|s^t_{sg}, s^t_{al}, s^{t-1}_{sg})P_B(s^{t-1}_{sg}|s^t_{sg}, s^t_{al}) \tag{6}$$

The space group forward and backward transition probabilities $P_F(s^t_{sg}|s^{t-1})$ and $P_B(s^{t-1}_{sg}|s^t)$ are parameterized by the multinoulli distribution defined by the logits output of the space group policy networks. The lattice parameters state s_{lp} transition probability is parameterized by the Gaussian distribution defined by the mean μ and variance σ^2. The atom fraction coordinates state s_{ac} transition probability is parameterized by the Multivariate Gaussian distribution given by the mean μ and covariance matrix Σ. The atom type state s_{at} transition probability is parameterized by the multinoulli distribution.

The sampling process is described in Algorithm 1. The lattice sampling process starts with the state s_0 which has lattice parameters as $a = b = c = 4, \alpha = \beta = \gamma = 90^o$, space group 1, empty crystal

graph at state s_0 $\mathscr{G}_{s_0}$. The state at any point, $s = (s_{sg}, s_{al})$, represents the crystal structure accumulated up to that step. Initially, at s_0, the crystal is empty. At each subsequent step t, the algorithm performs space group proposal and incremental construction. In the space group proposal, the high-level policy, θ_{sg}, proposes a new space group, s'_{sg}. This proposed space group governs the symmetry rules for the current step. It is used by the low-level policy, θ_{al}, to apply symmetry operations to the new reference atom being added. The choice of s'_{sg} can also impose new constraints on the crystal's lattice parameters, refining the overall structure. In the incremental construction, the low-level policy adds a new reference atom to the existing structure. The symmetry operations of the currently proposed space group, s'_{sg}, are applied to this new atom and all previously placed reference atoms in the structure. The resulting state at the end of the step, $s_t = (s'_{sg}, s'_{lp}, s'_{at}, s'_{ac})$, is an augmentation of the previous state, s_{t-1}. It incorporates the newly added atom (and its symmetric equivalents) and reflects the space group that is now governing the structure's symmetry. This step-by-step refinement ensures the DAG property of the generation process (more details in Appendix Sec. S2).

A key aspect of this sampling process is the implicit handling of Wyckoff positions. SHAFT does not require the explicit selection of a Wyckoff position. Instead, the low-level policy learns to place reference atoms at specific fractional coordinates. If these coordinates correspond to a special Wyckoff position for the given space group, the application of symmetry operations generates a set of symmetrically equivalent atoms, some of which will overlap. These overlapping sites are then merged using a standard distance tolerance (0.01 Å via the pymagen). If the coordinates correspond to a general Wyckoff position, a larger set of symmetrically equivalent atoms will be generated.

The policy is guided by a reward function that favors the generation of stable, low-energy structures. The policy learns to propose reference atom positions that result in favorable crystal structures, which may indirectly lead it to utilize Wyckoff positions commonly found in stable materials. This is an emergent behavior rather than an explicit design constraint.

The consistency between the space group, atom positions, and composition is maintained throughout this process. The atom positions are, by definition, consistent with the chosen space group because they are generated by its symmetry operations. The overall composition is managed incrementally. At each step, the model chooses an atom type, and a composition-related reward ($R_{comp}(x)$) guides the policy towards chemically valid structures. Furthermore, as shown in Algorithm 1, the choice of elements can be restricted using a validity mask based on compositional constraints, ensuring that the generated structures adhere to desired chemical formulas.

4.2 Physics-informed Reward Function

At the terminal state $x = s_{M_t}$ of the trajectory, a reward is returned by a non-negative function $R(x)$, providing feedback on the generated crystal structure, especially its validity and stability. To achieve these goals, we design the reward function to include the following key elements:

Algorithm 1 Hierarchical Trajectory Sampling

Input: Space group policy network θ_{sg}, atom policy network θ_a, lattice policy network θ_l, max step T, min lattice length min_l, max lattice length max_l, min lattice angle min_a, max lattice angle max_a

Return: Trajectory τ, complete crystal structure x

Initialize:

$s_{al} \leftarrow \{a = b = c = 4, \alpha = \beta = \gamma = 90^o\}$

$s_{sg} \leftarrow 1$

$\mathscr{G} \leftarrow \oslash$

Reference atom list $A_{ref} \leftarrow \oslash$

for step $t = 1$ **to** T **do**

    Set $p_{nsg} \leftarrow \theta_{sg}(s_{sg}, \mathscr{G})$.

    Space group $s'_{sg} \sim M_{nsg}(1, p_{nsg})$.

    Set $\alpha_{lattice}, \beta_{lattice}, \alpha_{atom}, \beta_{atom}, p_{ne} \leftarrow \theta_{sg}(s'_{sg}, s_{sg}, \mathscr{G})$

    Sample lattice parameters coefficient $w_a, w_b, w_c, w_\alpha, w_\beta, w_\gamma$ $\sim Beta(\alpha_{lattice}, \beta_{lattice})$

    Lattice parameters: $[a, b, c] = [w_a, w_b, w_c] * max_l + min_l$

    Lattice parameters: $[\alpha, \beta, \gamma] = [w_\alpha, w_\beta, w_\gamma] * max_a + min_a$

    An atom's fraction coordinate $(x, y, z) \sim Beta(\alpha_{atom}, \beta_{atom})$

    Get the atom's element valid *mask* based on the composition constraint.

    Set $p_{ne}[mask] = -\infty$.

    Atom's element $s'_{at} \sim M_{nsg}(1, p_{ne})$

    Set $A_{ref} = A_{ref} \cup (s'_{at}, s'_{ac},)$

    Add state $s'_{sg}, s'_{lp}, s'_{at}, s'_{ac}$ to trajectory τ

end for

The **formation energy term** dictates that a stable crystal structure will have a negative formation energy, thus defined as $R_e(x) = e^{-E(x)/T}$ where $E(x)$ is the predicted formation energy per atom given by the prediction model (Appendix Sec. S4.7), T is the normalization term.

The **bond length preferences term** R_b encourages the bond lengths of the input crystal structure to agree with the empirical lengths retrieved from the database. First, for each atom a_i in the crystal structure x, we search all its neighbors $nei(a_i)$ with the radius cutoff 4.0 Å. The neighbors can also include atoms from adjacent unit cells. We retrieve the minimum and average bond distance of all bond types existing in x from the Materials Project database (e.g. minimum bond distance of Li-O is 1.63 and the average bond distance of Li-O is 3.02). Then the difference between the bond length $d(a_i, a_j), a_j \in nei(a_i)$ with minimum $d_{min}(a_i, a_j)$ and average bond distance $d_{avg}(a_i, a_j)$ of (a_i, a_j) bond type.

$$R_{bond}(x) = \frac{|d(a_i, a_j) - d_{avg}(a_i, a_j)|}{n_{bond}}$$
$$+ e^{2(d_{min}(a_i, a_j) - d(a_i, a_j))} \quad (7)$$
$$\forall a_i \in x, \forall a_j \in nei(a_i)$$

where n_{bond} is the total number bond in the crystal structure x. We then regularize the bond term $R_{bond}(x)$ to $(0, 1)$ as $R_{bond}(x) = e^{-R_{bond}(x)}$.

The **density term** R_P encourages the structure density. Because the bond distance preference term applies a strict penalty for structures violating the minimum distance constraint, the generative model tends to generate a structure with long distances between

atom pairs with only a few neighbor atoms. This leads the model to generate gas with low density rather than solid-state density. On the other hand, structures with very high density (i.e. larger than 10) are unlikely to be realistic as the units are crowded with atoms causing a very high formation energy. We measure the generated structure density $P(x)$ (Appendix Sec. S4.5) and define the density term as the Gaussian function of structure density: $R_P(x) = ae^{\frac{-(P(x)-b)^2}{2c^2}}$.

The **composition validity term** is defined as $R_{comp}(x) = 1$ for valid composition and $R_{comp}(x) = 0$ otherwise. We follow composition validity given by the charge neutrality check [35]. Finally, the **physic-informed reward function** is composed as:

$$R(x) = w_e R_e(x) + w_p R_P(x) + w_b R_{bond}(x) + w_c R_{comp}(x) \quad (8)$$

where w_e, w_p, w_b, w_c are weighted scalar. We further discuss these terms in Appendix Sec.S4.4

4.3 State Representation

The crystal structure state must capture all relevant information about the crystal, including its atomic arrangement and the lattice parameters. We represent the crystal unit cell (L, A, X) described in Sec. 3.1 as a directed graph $\mathscr{G} = (\mathscr{V}, \mathscr{E})$ of node feature matrix $\mathscr{V}$ and edge matrix $\mathscr{E}$. The node features include the atom's atomic number and its fractional coordinates within the unit cell. The edges are determined by k-nearest neighbor with the maximum number of neighbors being 12 and the radius cut-off is 8.0 Å. The graph representation of the crystal structure is learned using a MatErials Graph Network (MEGNet) model [36] (details in Appendix Sec. S4.2) to satisfy the periodic invariance and E(3) invariance of crystal structure.

Lattice parameters are encoded using a multi-layer perceptron as:

$$h_{\mathscr{L}} = \text{MLP}([l_1, l_2, l_3, \sin(\alpha), \cos(\alpha), \sin(\beta), \cos(\beta),$$
$$\sin(\gamma), \cos(\gamma)]) \quad (9)$$

where l_1, l_2, l_3 are the lattice lengths, and α, β, γ are the angle of the lattice angle. The space group is encoded as h_{sg} using an embedding layer. Finally, the crystal structure state is simply $h_M = (h_{sg}, s_{al})$ where $h_{al} = [h_{\mathscr{G}}; h_{\mathscr{L}}]$. The encoded crystal structure state h_M is later used as the representation of the hierarchical state space s_M.

5 Experiments

Our SHAFT can be applied to any crystal discovery tasks given the set of elements. The main bottleneck is the prohibitive cost of validation of the generated structures. We will first focus on a constrained generation task with careful DFT validation (Sec. 5.1). Then we demonstrate the scalability of SHAFT on nearly unconstrained generation tasks (Sec. 5.3)

Baselines We compare our SHAFT with SOTA techniques including CDVAE [15], DiffCSP [20] and GFlowNets, which is a flat version of our method. CDVAE is a diffusion model that uses SE(3) equivariant GNNs adapted with periodicity. We train CDVAE, DiffCSP on the MP-Battery dataset for battery material discovery task (based

on requirements in Sec.5.1, more details in Appendix Sec. S5) and the MP-20 dataset[6] for general crystal generation (Sec. 5.3). We report the top-K (K=100) results ranked by Eq. 8. For CDVAE and DiffCSP, we sample 100 samples three times and report the mean and standard deviation. We follow the recent work on continuous GFlownet[37] to work on the continuous space of the atoms' coordinates and lattice parameters. The model has a single-level policy network that outputs space group, lattice parameters, atoms' coordinates, and atoms' type. Note that this is the first time GFlowNet has been applied successfully to complete crystal generation.

5.1 Constrained Generation: Battery Materials Discovery

For concreteness, we focus on battery material discovery, the most fundamental task in the battery industry worth hundreds of billions of dollars, and of great importance in securing a green energy future. The challenge is to generate stable structures with specific formulas and elements.

Motivated by the search for light-weight, transition-metal free cation materials, we explore the space of possible materials that can be made from the light elements Be, B, C, N, O, Si, P, S, and Cl, and one of the three alkali metals Li, Na and K. This space of materials constitutes materials that can be utilised in lithium-ion, sodium-ion, and potassium-ion battery materials, respectively. We discuss further the motivation of the experiments in Appendix S3.
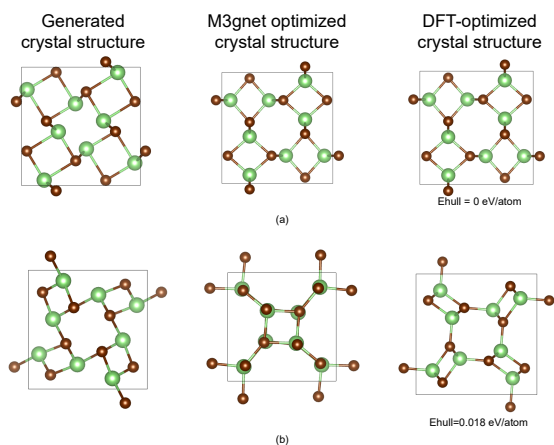

Fig. 3 Examples of two configurations of $(LiBr)_x$ generated by SHAFT and the corresponding structure optimized by M3GNet framework[38] and DFT.

5.1.1 Material Validity

We evaluate the proposed method and baseline methods on the validity of the generated crystal structure, measured based on two criteria. We follow the previous work[15] for validity measurements a) *structure validity*: a structure is valid as long as the minimum distance between any two atoms is more than 0.5 Å b) *composition validity*: a composition is valid if the overall charge computed by SMACT[35] is neutral. As seen in Tab. 1, both GFlowNet and SHAFT structure and composition validities are close to one, highlighting the effectiveness of learning reward-based exploration. The

Table 1 Validity of the generated structures. For SHAFT and GFlownet, we evaluate the top-K crystal structures ranked by the reward function after 8×10^5 states visited. For CDVAE and DiffCSP, we sample 100 structures.

Method	Structure ↑	Composition ↑
CDVAE	0.66±0.03	0.73±0.090
DiffCSP	0.86±0.03	0.59±0.005
GFlowNet	0.98±0.03	1.00±0.000
SHAFT	0.99±0.01	1.00±0.000

Table 2 Diversity of the generated structures. For SHAFT and GFlownet, we evaluate the top-K crystal structures ranked by the reward function after 8×10^5 states visited. For CDVAE and DiffCSP, we sample 100 structures.

Method	Crystal family ↑	Composition ↑	Structure ↑
CDVAE	0.15 ±0.09	1859.07 ±199.28	0.43 ±0.004
GFlowNet	1.97 ±0.15	165.13 ±32.55	0.84 ±0.03
DiffCSP	1.23 ±0.09	2360.97 ±110.37	0.57 ±0.06
SHAFT	2.19 ±0.06	147.80 ±15.81	0.89 ±0.05

structure and composition validities are used in the reward function described in Sec. 4.2. In contrast, CDVAE faces the common problem of sampling from data-induced distribution which is low structure validity.

5.1.2 Material Diversity

Following the previous works[15,39], we evaluate both the structure and composition diversity of the generated crystal structures. The *structure diversity* is defined as the average pairwise Euclidean distance between the structure fingerprint of any two generated materials[40]. The *composition diversity* is defined as the average pairwise distance between the composition fingerprints of any two generated materials[40]. More details are provided in S4.6. We further use the crystal family defined in Supplement Tab. 1 which is a group of space groups sharing some special geometric characteristics. The *crystal family diversity* is defined as the Shan-

Table 3 Average of formation energy and E_{hull} of the generated structures. For SHAFT and GFlownet, we evaluate the top-K crystal structures ranked by the reward function after 8×10^5 states visited. For CDVAE and DiffCSP, we sample 100 structures.

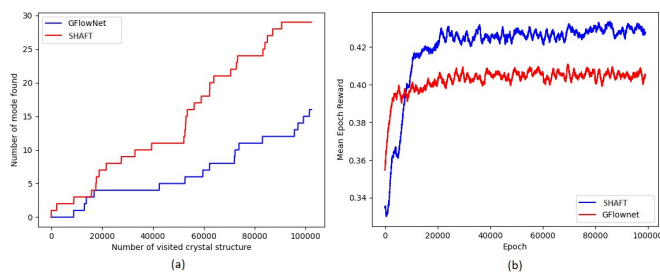| Method	Energy ↓	% energy < 0 ↑	E_{hull} ↓
CDVAE	-0.318±0.080	74.6±8.6	1.04 ±0.24
DiffCSP	0.120±0.108	45.5±6.3	0.55 ±0.04
GFlowNet	-1.014±0.003	98.6±1.6	0.32 ±0.02
SHAFT	-1.241±0.097	99.5±0.8	0.29 ±0.03

Fig. 4 (a) Comparison of SHAFT and GFlowNet in exploring crystal modes with max trajectory length $T = 3$
. A mode is defined as a valid crystal structure with negative formation energy. A step is an action of choosing one atom in the spacegroup-lattice-atom hierarchical state space. The number of visited states refers to the total number of candidate crystal structures generated and evaluated by the agent. (b) The average reward of crystal structures sampled by GFlownet and SHAFT in each epoch.

non–Wiener index[41] of the number of generated structures in each crystal family. We evaluate the diversity of structures discovered by the models and report the results in Tab. 2.

SHAFT demonstrates superior performance in generating a broad range of crystal families (Shannon-Wiener index of 2.19) and structurally distinct materials (structure diversity of 0.89), outperforming all baselines.

Conversely, for compositional diversity, we observe that the scores for GFlowNet (165.13) and SHAFT (147.80) are lower than those for CDVAE (1859.07) and DiffCSP (2360.97). This difference is an important and expected consequence of their fundamentally different generative approaches. CDVAE and DiffCSP are trained to replicate the distribution of the training data, and their high compositional diversity reflects the breadth of compositions present in the source dataset. In contrast, SHAFT and our GFlowNet baseline are reward-driven agents designed to actively seek out candidates that maximize a physics-informed reward function. This reward-guided exploration inherently focuses the search on compositional regions that yield high-reward structures—those with high stability and validity—within the constrained chemical space of the battery discovery task.

This represents a critical trade-off: while diffusion models may explore a wider range of compositions, this often comes at the cost of lower stability and validity, as shown by our results in Table 1 and Table 3. SHAFT, by design, prioritizes finding high-quality candidates within promising compositional niches, leading to a more targeted but less compositionally diverse set of outputs in this specific metric. This focus on high-reward regions is a key feature of our approach for efficient materials discovery, trading exhaustive compositional breadth for a higher yield of stable and valid material candidates.

5.1.3 Formation Energy

We also report the average formation energy and the percentage of structure with formation energy per atom smaller than 0 eV/atom, and energy above the hull. Compared with the flat GFlowNets,

our SHAFT find crystals with lower formation energy and more diversity in terms of crystal family and structure.

5.1.4 Modes Exploration

To evaluate the speed of exploring the material space and finding the valid material structures, we count the number of modes found by the generated crystal structures plotted against the number of states visited in Fig. 4a. We define a unique *mode* as a valid crystal structure satisfying four conditions. The first condition is three types of validity defined in Sec. 5.1. The second condition is that the crystal structure satisfies the minimum distance between any two atoms constraints. The third condition is that the structure must have negative formation energy. The fourth condition is that the composition cannot be the same as other modes.

As illustrated in Fig. 4a, SHAFT demonstrates significantly faster mode discovery than the baseline flat GFlowNet. This enhanced efficiency is a direct consequence of its hierarchical policy structure. The high-level policy, θ_{sg}, learns to strategically prune the vast search space by first proposing promising crystallographic space groups that are historically more likely to yield stable materials. This high-level decision provides a strong structural constraint. Consequently, the low-level policy, θ_{al}, is tasked with a more focused and tractable problem: arranging atoms and defining lattice parameters within that pre-selected, promising symmetric framework. By contrast, a flat GFlowNet must inefficiently explore all parameters simultaneously, making it slower to escape regions of the search space that lead to invalid or unstable structures. The discovery of nearly 30 unique modes after evaluating 10^5 candidates underscores the immense and sparse nature of the de novo materials design space. The vast majority of potential atomic combinations are unstable or physically invalid. The critical insight from this experiment is that SHAFT's hierarchical decomposition of the problem allows it to navigate this complex landscape more efficiently, identifying the rare, high-reward modes with substantially fewer samples than its non-hierarchical counterpart.

Diffusion models like CDVAE and DiffCSP are trained to be expert replicators, learning the distribution of known, stable materials from a database. Their ability to generate stable structures is largely inherited from this high-quality training data. In contrast, RL-based models like SHAFT are trained as systematic explorers, designed to search the entire chemical space to find novel, high-reward structures. This process necessarily involves learning from a large number of low-reward samples to map out the vast, unstable regions of the search space, thus again highlighting the immense and sparse nature of the de novo materials design space.

The average reward per epoch in Fig.4b shows that SHAFT not only speeds up the mode discovery but also discovers higher reward structures. The formation energy, bond length preferences, density, and composition validity term improving over epochs (see Fig.2) shows that the model can learn to embed the physical constraints into the policy network. Fig.3 showing the shift of the distribution of reward function terms from random initialization of an untrained SHAFT crystal structure to trained SHAFT further proves this point.
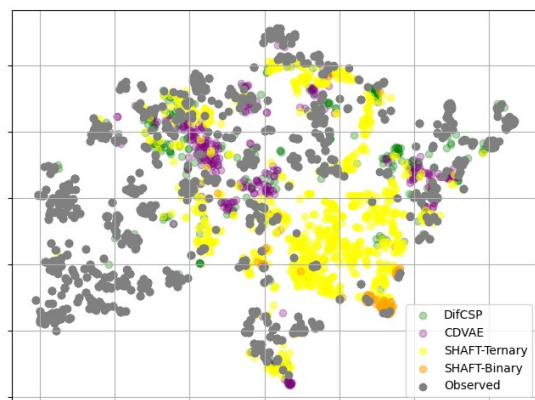
Fig. 5 Distributions of sampled crystal structure of observed crystal structure (MP-Battery dataset), DiffCSP, CDVAE, and SHAFT, plotted by t-SNE. SHAFT-Binary is binary crystal structures and SHAFT-Ternary is ternary crystal structures generated by SHAFT.
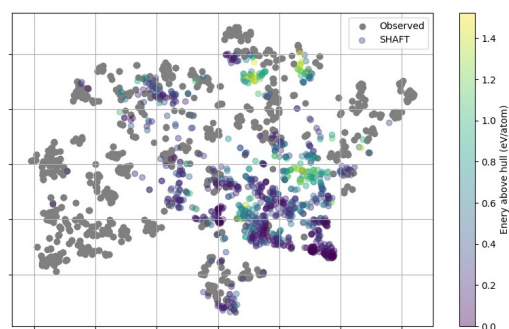

Fig. 6 Distributions of the sampled crystal structure of observed crystal structure (MP-Battery dataset) and SHAFT in term of energy above hull, plotted by t-SNE.

5.1.5 Novelty of sampled crystal structures

The advantage of SHAFT compared to the sampling-based methods such as CDVAE[15] or DiffCSP[20] is that it can easily explore and sample outside the distribution of observed or trained datasets due to the hierarchical guided-exploration. We performed a material space analysis of the training (MP-Battery) and generated structures, with t-distributed stochastic neighbor embedding (t-SNE)[42] in Fig.5 and 6. In Fig. 5, most crystal structures sampled by sampling-based methods are very near or overlapped with the observed dataset. On the other hand, SHAFT can explore and discover stable crystal structures (see Fig. 6) outside the dataset distribution and discover stable materials in these out-of-distribution regions.

5.1.6 Stability of Generated Materials

It is a common practice to relax the generated crystal structures to seek the lower potential energy surface using DFT calculation iteratively. As DFT calculation is expensive, it is desirable to generate a

Table 4 Match rates of the generated crystal paired with structures optimized by M3GNet [38]

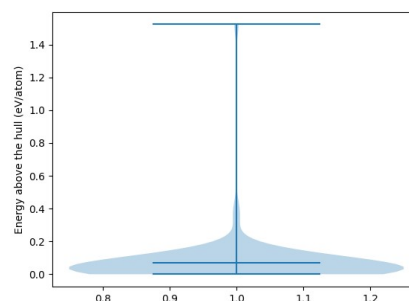| Methods	Match rate ↑	RMS displacement ↓
CDVAE	0.46 ±0.03	0.287 ±0.0133
DiffCSP	0.33 ±0.04	0.335 ±0.041
GFlowNet	0.80 ±0.01	0.174 ±0.019
SHAFT	0.82 ±0.02	0.161 ±0.020

Fig. 7 The distribution of energy above the hull of DFT optimized structures. Most of the generated are stable ($E_{hull} = 0eV/atom$) or metastable $E_{hull} < 0.05eV/atom$. We can achieve low E_{hull} without optimizing directly.

structure that is close to the energy minima. In this experiment, we compare the generated crystal structure with its optimized structure. We use the M3GNet framework[38] to iteratively optimize the energy predicted by the potential surface energy model. Examples of generated structures and their corresponding optimized structures are shown in Fig. 3.

Match rate We follow the previous work in[39] to evaluate the match rate of crystal structure relaxation. A structure m and its optimized structure m' are matched if their atoms' translation and angle are within tolerance thresholds, indicating that the generated structure is close to the optimal, and thus is more stable. We use the matching algorithm provided by pymatgen library[43] in StructureMacher with 10° angle tolerance, 1.0 fractional length tolerance, and 1.0 site tolerance. The match rate is the fraction of the number of matched structures on the total number of generated structures.

The results reported in Tab. 4 show that our proposed method can produce more structures (at the rate of 0.82) that are nearly optimal in terms of total energy compared to GFlowNets and CDVAE.

We also report the match rate of structures generated by SHAFT and their DFT-optimized structures (reported in Sec. 5.1.7) instead of M3GNet-optimized structures. In stark contrast, when comparing the as-generated structures to their DFT-relaxed ground truths, the match rate drops to 0.042 and the RMS displacement increases to 0.297 Å.

This discrepancy is expected and highlights a key characteristic of surrogate-model-guided generation. The high match rate with M3GNet-relaxed structures validates that SHAFT effectively optimizes its outputs for its given reward function—the M3GNet

potential energy surface (PES). The model learns to produce structures that are already near a local minimum on this surrogate PES.

However, the M3GNet potential, while highly accurate, is an approximation of the true quantum mechanical landscape described by DFT. The lower match rate with DFT-relaxed structures quantifies the inherent gap between the surrogate model and the ground truth. The larger structural rearrangement required during DFT optimization is a necessary step to move the structure from the surrogate's predicted minimum to the true ground-state configuration. This also illustrates a common challenge known as "reward hacking": the model becomes highly proficient at generating structures that minimize the energy of the surrogate M3GNet potential, which is an accurate but imperfect proxy for the true quantum mechanical landscape described by DFT.

Ultimately, this analysis reinforces the power of the hierarchical generation and validation workflow. SHAFT, guided by the M3GNet surrogate, is exceptionally effective at identifying promising regions of the vast chemical space that contain verifiably stable materials. The results confirm that while a final DFT refinement is essential for achieving ground-truth accuracy, SHAFT's approach is highly successful for the critical initial discovery phase.

5.1.7 DFT Validation

We sample and choose the top-K generated materials for DFT verification. Out of 100 crystal structures, 95% (95) are successfully optimized. The complete list of DFT-optimized structures is included in the Supplement material Github. Fig.7 shows that most DFT-optimized structures are stable or metastable ($E_{hull} < 0.05eV/atom$). The generated and optimized structures with their total energy per atom, E_{hull}, and further results and calculation details are available in the Appendix.

5.2 Generating stable structure with target property

Our proposed framework SHAFT offers the flexibility to optimize multiple objectives via the reward function. We experiment to generate stable structures with low band gap. The experiment setup is similar to the battery material discovery task (Sec.5). While the ideal band gap depends on the specific battery component, a low or zero band gap is highly advantageous for electrode materials. High electronic conductivity is critical for enabling fast charge-transfer kinetics and improving charge/discharge rates, and thus by targeting a near-zero band gap in this experiment, our goal is to discover novel candidates for battery electrodes. We add the following band gap term for the near zero band gap constraint:

$$R_{bg}(x) = a_{bg}e^{\frac{-(P_{bg}(x)-b_{bg})^2}{2c_{bg}^2}} \qquad (10)$$

where $a_{bg} = 3.0$, $b_{bg} = 0.0$, $c_{bg} = 0.5$. Then the reward function is defined as:

$$R(x) = w_eR_e(x) + w_{bg}R_{bg}(x) + w_pR_P(x) + w_bR_{bond}(x) + w_cR_{comp}(x) \qquad (11)$$

We set weights as $w_e = w_{bg} = 0.1$, $w_p = 0.1$, $w_b = 0.5$, and $w_c = 0.1$. To demonstrate that the generated structures are stable and have near zero band gap, we present the average of formation and band

gap in Tab.5.

Table 5 Average of formation energy and band gap of the generated structures. For SHAFT and GFlownet, we evaluate the top-K crystal structures ranked by the reward function after 8×10^5 states visited. For CDVAE and DiffCSP, we sample 100 structures.

Method	Energy ↓	% energy < 0 ↑	Band gap ↓
CDVAE	-0.82	83.33	0.45
DiffCSP	-0.96	86.74	0.48
GFlowNet	-0.63	90.91	0.08
SHAFT	-0.84	100.00	0.04

5.3 Exploring a Very Large Element Space

Table 6 The diversity experiment results of CDVAE, GFlownet, and SHAFT on 89 elements

Methods	Crystal family diversity ↑	Composition diversity ↑	Structure diversity ↑
CDVAE	0.95	1857.31	0.74
DiffCSP	2.60	1812.25	0.93
GFlownet	2.37	1399.59	0.99
SHAFT	2.32	1471.59	1.01

Table 7 The validity, energy, and stability experiment results of CDVAE, GFlownet and SHAFT on 89 elements

Methods	Comp. val.	Struct. val.	Avg. Form. E.	% E. < 0	Match rate ↑	RMS dis. ↓
CDVAE	0.86	1.00	-0.84	58	0.71	0.14
DiffCSP	0.83	1.00	-0.85	90	0.94	0.06
GFlownet	1.00	1.00	-0.89	72	0.66	0.18
SHAFT	1.00	0.97	-1.14	87	0.71	0.19

To further demonstrate the ability to generalize to the whole chemical space, we train our proposed method on 89 elements from H to Pu. Because we have 89 instead of 12 elements, the composition diversity is higher than the experiment in Tab. 2. As shown in Tab.7 and 6, our proposed method maintains a high percentage of stable structure and low formation energy.

6 Conclusion

We have proposed SHAFT, a Hierarchical Generative Flow Network for crystal structure generation, aiming at rapid exploration of the exponential crystal space and simultaneously satisfying physics constraints. SHAFT is built on a hierarchical state space, allowing for multi-level policy networks to operate on action abstraction. It effectively exploits the high-symmetry in the crystal structure space, defining space transformation groups. The framework is flexible for domain experts to embed domain knowledge to guide the generation process through space structure design and reward

engineering. SHAFT demonstrates its superiority in efficiency in exploration, diversity, and stability in the generated crystal structures.

While this work has primarily focused on generating stable crystal structures with desirable formation energies and targeted band gaps, the SHAFT framework offers inherent flexibility for broader applications in materials discovery. In principle, additional material properties, such as mechanical characteristics (e.g., hardness, elastic moduli) or specific optical responses (e.g., refractive index, absorption spectra), could be seamlessly integrated into the generative process. This would typically involve incorporating corresponding terms into the reward function, guided by accurate and computationally efficient surrogate models capable of predicting these properties from structural inputs. However, expanding to multiple target properties introduces further considerations. The primary challenge lies in navigating the complexities of multi-objective optimization, particularly when objectives are conflicting, which may necessitate sophisticated strategies beyond simple weighted-sum approaches to effectively explore the Pareto front[44]. Furthermore, the computational overhead of evaluating an increasing number of property predictors must be carefully managed to maintain the efficiency of the generation process. Future work could explore advanced multi-objective SHAFT algorithms and the development of robust surrogate models for a wider range of material characteristics to fully exploit SHAFT's potential in designing novel, multi-functional materials.

Conflicts of interest

There are no conflicts to declare.

Data Availability Statement

The implementation and data (MP-Battery, sampled crystal structures, and their DFT-optimized structures) are available at https://github.com/ngminhtri0394/SHAFT and 10.5281/zenodo.17014637.

References

1 L. I. Berger, *Semiconductor Materials*, CRC Press, 2020.

2 J. Noh, J. Kim, H. S. Stein, B. Sanchez-Lengeling, J. M. Gregoire, A. Aspuru-Guzik and Y. Jung, *Matter*, 2019, **1**, 1370–1384.

3 M. J. Mehl, D. Hicks, C. Toher, O. Levy, R. M. Hanson, G. Hart and S. Curtarolo, *Computational Materials Science*, 2017, **136**, S1–S828.

4 D. Hicks, M. J. Mehl, E. Gossett, C. Toher, O. Levy, R. M. Hanson, G. Hart and S. Curtarolo, *Computational Materials Science*, 2019, **161**, S1–S1011.

5 D. Hicks, M. J. Mehl, M. Esters, C. Oses, O. Levy, G. L. Hart, C. Toher and S. Curtarolo, *Computational Materials Science*, 2021, **199**, 110450.

6 A. Jain, S. P. Ong, G. Hautier, W. Chen, W. D. Richards, S. Dacek, S. Cholia, D. Gunter, D. Skinner, G. Ceder and K. A. Persson, *APL Materials*, 2013, **1**, 1–12.

7 J. J. Irwin and B. K. Shoichet, *Journal of Chemical Information and Modeling*, 2005, **45**, 177–182.

8 S. Chithrananda, G. Grand and B. Ramsundar, Machine Learning for Molecules Workshop, NeurIPS, Online, 2020.

9 Y. Liu, M. Ott, N. Goyal, J. Du, M. Joshi, D. Chen, O. Levy, M. Lewis, L. Zettlemoyer, V. Stoyanov and P. G. Allen, *arXiv preprint arXiv:1907.11692*, 2019.

10 M. AI4Science, A. Hernandez-Garcia, A. Duval, A. Volokhova, Y. Bengio, D. Sharma, P. L. Carrier, Y. Benabed, M. Koziarski and V. Schmidt, 2023.

11 A. Belkly, M. Helderman, V. L. Karen and P. Ulkch, *Acta crystallographica. Section B, Structural science*, 2002, **58**, 364–369.

12 G. Hautier, C. Fischer, V. Ehrlacher, A. Jain and G. Ceder, *Inorganic Chemistry*, 2011, **50**, 656–663.

13 H. C. Wang, S. Botti and M. A. Marques, *npj Computational Materials 2021 7:1*, 2021, **7**, 1–9.

14 L. Wei, N. Fu, E. M. Siriwardane, W. Yang, S. S. Omee, R. Dong, R. Xin and J. Hu, *Inorganic Chemistry*, 2022, **61**, 8431–8439.

15 T. Xie, X. Fu, O.-E. Ganea, R. Barzilay and T. Jaakkola, Proceeding of International Conference on Learning Representations, 2022.

16 C. J. Court, B. Yildirim, A. Jain and J. M. Cole, *Journal of Chemical Information and Modeling*, 2020, **60**, 4518–4535.

17 Y. Zhao, M. Al-Fahdi, M. Hu, E. M. D Siriwardane, Y. Song, A. Nasiri, J. Hu, Y. Zhao, E. M. D Siriwardane, Y. Song, A. Nasiri, J. Hu, M. Al-Fahdi and M. Hu, *Advanced Science*, 2021, **8**, 2100566.

18 S. Kim, J. Noh, G. H. Gu, A. Aspuru-Guzik and Y. Jung, *ACS Central Science*, 2020, **6**, 1412–1420.

19 Y. Luo, C. Liu and S. Ji, Proceedings of Conference on Neural Information Processing Systems, 2023.

20 R. Jiao, W. Huang, P. Lin, J. Han, P. Chen, Y. Lu and Y. Liu, Proceedings of the Advances in Neural Information Processing Systems, 2023.

21 D. Levy, S. S. Panigrahi, S.-O. Kaba, Q. Zhu, M. Galkin, S. Miret and S. Ravanbakhsh, The AI for Accelerated Materials Discovery (AI4Mat) Workshop, 2024.

22 A. Merchant, S. Batzner, S. S. Schoenholz, M. Aykol, G. Cheon and E. D. Cubuk, *Nature*, 2023, **624**, 80–85.

23 C. Zeni, R. Pinsler, D. Zügner, A. Fowler, M. Horton, X. Fu, A. Shysheya, J. Crabbé, L. Sun, J. Smith, B. Nguyen, H. Schulz, S. Lewis, C.-W. Huang, Z. Lu, Y. Zhou, H. Yang, H. Hao, J. Li, R. Tomioka and T. Xie, 2023.

24 E. Zamaraeva, C. M. Collins, D. Antypov, V. V. Gusev, R. Savani, M. S. Dyer, G. R. Darling, I. Potapov, M. J. Rosseinsky and P. G. Spirakis, *Digital Discovery*, 2023.

25 O. Nachum, G. Brain, S. Gu, H. Lee and S. Levine, Conference on Neural Information Processing Systems, 2018.

26 Z. Wen DeepMind, D. Precup DeepMind, M. Ibrahimi DeepMind, A. Barreto DeepMind, B. Van Roy DeepMind and S. Singh DeepMind, Conference on Neural Information Processing Systems, 2020.

27 E. Bengio, M. Jain, M. Korablyov, D. Precup and Y. Bengio, *Advances in Neural Information Processing Systems*, 2021, **33**, 27381–27394.

28 M. Jain, E. Bengio, A.-H. Garcia, J. Rector-Brooks, B. F. P. Dossou, C. Ekbote, J. Fu, T. Zhang, M. Kilgour, D. Zhang,

L. Simine, P. Das and Y. Bengio, *Proceeding of International Conference on Machine Learning*, 2022.

29 T. Deleu, A. Góis, C. Emezue, M. Rankawat, S. Lacoste-Julien, S. Bauer and Y. Bengio, Proceedings of the Conference on Uncertainty in Artificial Intelligence, 2022.

30 Y. Li, S. Luo, H. Wang and J. HAO, *CFlowNets: Continuous control with Generative Flow Networks*, 2023.

31 Jiangyan Ma, Emmanuel Bengio, Yoshua Bengio and Dinghuai Zhang, NeurIPS AI for Science Workshop, 2023.

32 Minsu Kim, Taeyoung Yun, Emmanuel Bengio, Dinghuai Zhang, Yoshua Bengio, Sungsoo Ahn and Jinkyoo Park, Proceeding of International Conference on Learning Representations, 2024.

33 M. Glazer, G. Burns and A. N. Glazer, *Space groups for solid state scientists*, 2012.

34 N. Malkin, M. Jain, E. Bengio, C. Sun and Y. Bengio, Proceedings of Advances in Neural Information Processing Systems, 2022.

35 D. Davies, K. Butler, A. Jackson, J. Skelton, K. Morita and A. Walsh, *Journal of Open Source Software*, 2019, **4**, 1361.

36 C. Chen, W. Ye, Y. Zuo, C. Zheng and S. P. Ong, *Chemistry of Materials*, 2019, **31**, 3564–3572.

37 S. Lahlou, T. Deleu, P. Lemos, D. Zhang, A. Volokhova, A. Hernández-García, L. Néhale Ezzine, Y. Bengio and N. Malkin, Proceedings of the International Conference on Machine Learning, 2023.

38 C. Chen and S. P. Ong, *Nature Computational Science 2022 2:11*, 2022, **2**, 718–728.

39 Y. Zhao, E. M. Siriwardane, Z. Wu, N. Fu, M. Al-Fahdi, M. Hu and J. Hu, *npj Computational Materials 2023 9:1*, 2023, **9**, 1–12.

40 H. Pan, A. M. Ganose, M. Horton, M. Aykol, K. A. Persson, N. E. Zimmermann and A. Jain, *Inorganic Chemistry*, 2021, **60**, 1590–1603.

41 C. E. Shannon, *Bell System Technical Journal*, 1948, **27**, 379–423.

42 Laurens van der Maaten and Geoffrey Hinton, *Journal of Machine Learning Research*, 2008, **9**,.

43 S. P. Ong, W. D. Richards, A. Jain, G. Hautier, M. Kocher, S. Cholia, D. Gunter, V. L. Chevrier, K. A. Persson and G. Ceder, *Computational Materials Science*, 2013, **68**, 314–319.

44 M. Jain, S. C. Raparthy, A. Hernandez-Garcia, J. Rector-Brooks, Y. Bengio, S. Miret and E. Bengio, Proceedings of the 40th International Conference on Machine Learning, 2023.

Data Availability Statement

September 1, 2025

The implementation and data (MP-Battery, sampled crystal structures, and their DFT-optimized structures) are available at https://github.com/ngminhtri0394/SHAFT and 10.5281/zenodo.17014637.

1